A rigorous approach to study kinetic and 3D effects on resistive wall mode

Yueqiang Liu[1] **and F. Villone**[2]

[1]Euratom/UKAEA Fusion Association, Culham Science Centre, Abingdon, OX14 3DB, UK

[2]ENEA/CREATE, DAEIMI, Universita di Cassino, Via di Biasio 43, Cassino (FR), Italy

E-mail: yueqiang.liu@ukaea.org.uk

Abstract. A self-consistent, rigorous approach is proposed to study the synergistic effects of plasma flow, drift kinetic resonances and three-dimensional conducting structures on the resistive wall mode. This approach is based on coupling between the hybrid MHD-kinetic computation and the 3D electromagnetic eddy current computation via a specific boundary condition. It allows study of the stability and feedback control of the resistive wall mode, as well as the resonant field amplification associated with the stable mode response. A test example is considered to show the combined effects of plasma flow, kinetic effects, and 3D conductors on the mode stability.

PACS numbers: 52.35.Py, 28.52.Av, 52.55.Fa, 52.65.Kj

Submitted to: *Plasma Phys. Control. Fusion*

1. Introduction

Adequate modelling of the RWM in present experiments, or in ITER, requires consideration of two important factors. One are the physics factors involved in the mode damping, such as the effects of plasma toroidal flow, the drift kinetic resonances of the mode with the plasma particle species. The other is the geometrical factor; mostly the effects of 3D external conducting structures (resistive walls, coils, supporting structures, etc.) on the mode stability and control.

The importance of both above mentioned factors have been appreciated recently, and toroidal numerical codes have been developed in both directions. For instance, the MARS-K code [1] has recently been developed to study the drift kinetic effects on the passive stability of the RWM, assuming a 2D (i.e. axi-symmetric), complete thin shell approximation for the resistive walls. The code is based on the single fluid MHD code MARS-F [2], which includes the toroidal plasma flow and MHD type of continuum damping physics. Another example of MHD codes with the inclusion of flow damping physics is the CASTOR-FLOW code [3], which also treats the external conducting structures in a 2D manner. On the other hand, several codes have been developed to model the RWM stability and control with 3D conductors. These include CarMa [4, 5], VALEN [6], and STARWALL [7]. In particular, the importance of 3D wall effects has been demonstrated by a quantitative comparison of the CarMa modelling results with the experimental measurements in RFX for the RWM growth rates [8]. However, so far all the codes with 3D walls assume an ideal, mass-free description for the plasma, with no proper (if any) plasma flow and kinetic effects included.

In this work, we report a new implementation of the CarMa code, which couples the MARS-K code and the 3D electromagnetic code CARIDDI [9], based on a backward coupling scheme proposed in [10]. We extended this coupling scheme to include the feedback coils in a suitable and efficient way, in order to model the resonant field amplification (RFA) and the RWM feedback stabilisation in the presence of 3D conductors. We note that this coupling scheme is not specific to the CarMa code. It can be adapted to couple any 3D eddy current solver with a (possibly non-linear) MHD solver.

The next Section gives a detailed description of the backward coupling procedure in the presence of coils, followed by a Section reporting the CarMa results for a test equilibrium, where the plasma flow and kinetic effects, from one side, and the effects of 3D walls, from the other side, are both included in the simulation. More comprehensive modelling for realistic plasmas, such as the RFA simulation in JET with 3D walls, and the RWM control in ITER with 3D walls and plasma flow, will be carried out in the future work.

2. Coupling strategy

2.1. Boundary condition

In order to couple a MHD (or MHD-kinetic hybrid) code that computes the plasma dynamics, with an electromagnetic code that solves for the eddy currents in conducting structures, we introduce a coupling surface, which is located between the plasma surface and the nearest conducting structures outside the plasma, with otherwise arbitrarily chosen shape and radial position. The backward coupling scheme [10] consists of the following two steps. First, we run the eddy current code to compute the response of 3D structures to a given coil current $\mathbf{I}_f$ (the 3D coil geometry, such as finite extensions and gaps along the toroidal angle, complicated coil winding in some cases, also enters into the field computation), and to a set of unit perturbations from the plasma itself. The unit perturbations from the plasma are defined on the coupling surface, and represented by an equivalent surface current perturbation $\mathbf{I}_{\rm eqv}$, defined on the same coupling surface. In other words, the plasma response field, outside the coupling surface, is completely represented by the field generated by the equivalent surface current $\mathbf{I}_{\rm eqv}$ [4]. At the second step, we compute the normal $\mathbf{b}_N$ and and the tangential $\mathbf{b}_T$ components of the *total* perturbed field, defined on the coupling surface and composed of contributions from the plasma (the equivalent surface current $\mathbf{I}_{\rm eqv}$), the 3D eddy currents from 3D structures, and the coil current $\mathbf{I}_f$. A relation between $\mathbf{b}_N$, $\mathbf{b}_T$ and $\mathbf{I}_f$ is then used as the boundary condition for the MHD code, in order to carry out the stability, RFA response, or feedback computations. The coupling surface serves the computational boundary of the final MHD problem, with inertial, flow, and kinetic effects included.

We emphasise that, in principle, the 3D coils can be treated as part of the conducting structures. Our isolation of the coils contribution from 3D conductors is motivated by physics applications, such as the RFA analysis and the feedback study.

In the following, we describe rigorously the above procedure in terms of discretised quantities (matrices and vectors), which are more relevant for the purpose of the numerical implementation, although it is also possible to recast this procedure in the continuous from (functions and linear operators).

We assume that the solution field of the MHD perturbation is decomposed in total number of M Fourier harmonics along the poloidal angle (we consider only a single toroidal mode number n). The *total* perturbed magnetic field at the coupling surface, $\mathbf{b}_N$ and $\mathbf{b}_T$, become two vectors of dimension $M \times 1$. Following notations in [10], we write the eddy current equation for the 3D structures in a circuit-like form

$$\overleftrightarrow{\mathbf{R}}\mathbf{I} + \gamma\overleftrightarrow{\mathbf{L}}\mathbf{I} = -\gamma\overleftrightarrow{\mathbf{M}}\mathbf{I}_{\rm eqv} - \gamma\overleftrightarrow{\mathbf{M}}_f\mathbf{I}_f, \tag{1}$$

where $\mathbf{I}$ is the eddy current in the structures - the solution vector of dimension $N \times 1$ of the eddy current solver. The resistance matrices $\overleftrightarrow{\mathbf{R}}$ and the self-inductance matrices $\overleftrightarrow{\mathbf{L}}$ of the structures have a dimension $N \times N$. The RHS terms of equation (1) correspond to the voltages generated by the plasma response and the coil current, and applied to the conducting structures, hence $\overleftrightarrow{\mathbf{M}}$ and $\overleftrightarrow{\mathbf{M}}_f$ represent the mutual inductance matrices

between the equivalent surface current $\mathbf{I}_{\rm eqv}$ and the coil current $\mathbf{I}_f$ respectively. The dimension of $\mathbf{I}_{\rm eqv}$ is $M \times 1$, since this current is also decomposed in poloidal Fourier harmonics. [The surface current $\mathbf{I}_{\rm eqv}$ has both poloidal and toroidal components, one of which can be eliminated by the divergence-free condition.] The dimension of $\mathbf{I}_f$ is $K \times 1$, with K being the total number of feedback (or antenna) coils. Consequently, the dimensions of matrices $\overleftrightarrow{\mathbf{M}}$ and $\overleftrightarrow{\mathbf{M}}_f$ are $N \times M$ and $N \times K$ respectively. γ from Eq. (1) is the eigenvalue that we determine while solving the final stability or feedback problem. For a forcing problem like in the RFA computation, where $\mathbf{I}_f$ is a given source term (antenna), $\gamma \equiv i\omega_{\rm ext}$ is a given complex number, with $\omega_{\rm ext}$ being the (real) excitation frequency of the source term.

The normal and tangential components of the total magnetic fields on the coupling surface can be computed as

$$\mathbf{b}_N = \overleftrightarrow{\mathbf{S}}_1\mathbf{I} + \overleftrightarrow{\mathbf{S}}_2\mathbf{I}_{\rm eqv} + \overleftrightarrow{\mathbf{S}}_3\mathbf{I}_f, \tag{2}$$

$$\mathbf{b}_T = \overleftrightarrow{\mathbf{P}}_1\mathbf{I} + \overleftrightarrow{\mathbf{P}}_2\mathbf{I}_{\rm eqv} + \overleftrightarrow{\mathbf{P}}_3\mathbf{I}_f, \tag{3}$$

where $\overleftrightarrow{\mathbf{S}}_j$ and $\overleftrightarrow{\mathbf{P}}_j$ are mutual inductance matrices between the corresponding currents and the coupling surface. Note that $\mathbf{b}_T$ actually have two components (poloidal and toroidal). In practice, it is sufficient to use one of them, in combination with the normal component $\mathbf{b}_N$, to obtain the boundary condition for the final MHD solver. For definiteness, we will assume that $\mathbf{b}_T$ denotes the poloidal component of the total field.

Since the core MHD equations with flow is normally formulated as a *linear* eigenvalue problem (linear stability problem), it is highly desirable to formulate the final boundary condition, a relation between $\mathbf{b}_N$, $\mathbf{b}_T$ and $\mathbf{I}_f$, in a linear form of the eigenvalue γ. This idea has been proposed by several authors recently [11, 10, 12]. Our following derivation will show that it is indeed possible to obtain such a linear boundary condition.

Combining Eqs. (1) and (2) by eliminating $\mathbf{I}_{\rm eqv}$, we have

$$-\gamma\left(\overleftrightarrow{\mathbf{L}} - \overleftrightarrow{\mathbf{M}}\overleftrightarrow{\mathbf{S}}_2^{-1}\overleftrightarrow{\mathbf{S}}_1\right)^{-1}\overleftrightarrow{\mathbf{M}}\overleftrightarrow{\mathbf{S}}_2^{-1}\mathbf{b}_N = \left(\overleftrightarrow{\mathbf{L}} - \overleftrightarrow{\mathbf{M}}\overleftrightarrow{\mathbf{S}}_2^{-1}\overleftrightarrow{\mathbf{S}}_1\right)^{-1}\overleftrightarrow{\mathbf{R}}\mathbf{I} + \gamma\mathbf{I} + \gamma\left(\overleftrightarrow{\mathbf{L}} - \overleftrightarrow{\mathbf{M}}\overleftrightarrow{\mathbf{S}}_2^{-1}\overleftrightarrow{\mathbf{S}}_1\right)^{-1}\left(\overleftrightarrow{\mathbf{M}}_f - \overleftrightarrow{\mathbf{M}}\overleftrightarrow{\mathbf{S}}_2^{-1}\overleftrightarrow{\mathbf{S}}_3\right)\mathbf{I}_f. \tag{4}$$

Similarly, combining Eqs. (1) and (3) gives

$$-\gamma\left(\overleftrightarrow{\mathbf{L}} - \overleftrightarrow{\mathbf{M}}\overleftrightarrow{\mathbf{P}}_2^{-1}\overleftrightarrow{\mathbf{P}}_1\right)^{-1}\overleftrightarrow{\mathbf{M}}\overleftrightarrow{\mathbf{P}}_2^{-1}\mathbf{b}_T = \left(\overleftrightarrow{\mathbf{L}} - \overleftrightarrow{\mathbf{M}}\overleftrightarrow{\mathbf{P}}_2^{-1}\overleftrightarrow{\mathbf{P}}_1\right)^{-1}\overleftrightarrow{\mathbf{R}}\mathbf{I} + \gamma\mathbf{I} + \gamma\left(\overleftrightarrow{\mathbf{L}} - \overleftrightarrow{\mathbf{M}}\overleftrightarrow{\mathbf{P}}_2^{-1}\overleftrightarrow{\mathbf{P}}_1\right)^{-1}\left(\overleftrightarrow{\mathbf{M}}_f - \overleftrightarrow{\mathbf{M}}\overleftrightarrow{\mathbf{P}}_2^{-1}\overleftrightarrow{\mathbf{P}}_3\right)\mathbf{I}_f. \tag{5}$$

Subtracting Eq. (4) by Eq. (5), we obtain

$$\gamma[(\overleftrightarrow{\mathbf{L}} - \overleftrightarrow{\mathbf{M}}\overleftrightarrow{\mathbf{P}}_2^{-1}\overleftrightarrow{\mathbf{P}}_1)^{-1}\overleftrightarrow{\mathbf{M}}\overleftrightarrow{\mathbf{P}}_2^{-1}\mathbf{b}_T - (\overleftrightarrow{\mathbf{L}} - \overleftrightarrow{\mathbf{M}}\overleftrightarrow{\mathbf{S}}_2^{-1}\overleftrightarrow{\mathbf{S}}_1)^{-1}\overleftrightarrow{\mathbf{M}}\overleftrightarrow{\mathbf{S}}_2^{-1}\mathbf{b}_N] = \overleftrightarrow{\mathbf{L}}_1\mathbf{I} + \gamma\overleftrightarrow{\mathbf{L}}_2\mathbf{I}_f, \tag{6}$$

where

$$\overleftrightarrow{\mathbf{L}}_1 = \left(\overleftrightarrow{\mathbf{L}} - \overleftrightarrow{\mathbf{M}}\overleftrightarrow{\mathbf{S}}_2^{-1}\overleftrightarrow{\mathbf{S}}_1\right)^{-1}\overleftrightarrow{\mathbf{R}} - \left(\overleftrightarrow{\mathbf{L}} - \overleftrightarrow{\mathbf{M}}\overleftrightarrow{\mathbf{P}}_2^{-1}\overleftrightarrow{\mathbf{P}}_1\right)^{-1}\overleftrightarrow{\mathbf{R}}, \tag{7}$$

and

$$\overleftrightarrow{\mathbf{L}}_2 = \left(\overleftrightarrow{\mathbf{L}} - \overleftrightarrow{\mathbf{M}}\overleftrightarrow{\mathbf{S}}_2^{-1}\overleftrightarrow{\mathbf{S}}_1\right)^{-1}\left(\overleftrightarrow{\mathbf{M}}_f - \overleftrightarrow{\mathbf{M}}\overleftrightarrow{\mathbf{S}}_2^{-1}\overleftrightarrow{\mathbf{S}}_3\right) - \left(\overleftrightarrow{\mathbf{L}} - \overleftrightarrow{\mathbf{M}}\overleftrightarrow{\mathbf{P}}_2^{-1}\overleftrightarrow{\mathbf{P}}_1\right)^{-1}\left(\overleftrightarrow{\mathbf{M}}_f - \overleftrightarrow{\mathbf{M}}\overleftrightarrow{\mathbf{P}}_2^{-1}\overleftrightarrow{\mathbf{P}}_3\right) \quad (8)$$

Equations (2) and (3) can also be combined to eliminate $\mathbf{I}_{\text{eqv}}$, yielding

$$\overleftrightarrow{\mathbf{S}}_2^{-1}\mathbf{b}_N - \overleftrightarrow{\mathbf{P}}_2^{-1}\mathbf{b}_T = \left(\overleftrightarrow{\mathbf{S}}_2^{-1}\overleftrightarrow{\mathbf{S}}_1 - \overleftrightarrow{\mathbf{P}}_2^{-1}\overleftrightarrow{\mathbf{P}}_1\right)\mathbf{I} + \left(\overleftrightarrow{\mathbf{S}}_2^{-1}\overleftrightarrow{\mathbf{S}}_3 - \overleftrightarrow{\mathbf{P}}_2^{-1}\overleftrightarrow{\mathbf{P}}_3\right)\mathbf{I}_f. \quad (9)$$

Finally, by eliminating the quantity $\mathbf{I}$ from Eqs. (6) and (9), we arrive at

$$\begin{aligned}
&\left[\overleftrightarrow{\mathbf{S}}_2^{-1} + \gamma\left(\overleftrightarrow{\mathbf{S}}_2^{-1}\overleftrightarrow{\mathbf{S}}_1 - \overleftrightarrow{\mathbf{P}}_2^{-1}\overleftrightarrow{\mathbf{P}}_1\right)\overleftrightarrow{\mathbf{L}}_1^{-1}\left(\overleftrightarrow{\mathbf{L}} - \overleftrightarrow{\mathbf{M}}\overleftrightarrow{\mathbf{S}}_2^{-1}\overleftrightarrow{\mathbf{S}}_1\right)^{-1}\overleftrightarrow{\mathbf{M}}\overleftrightarrow{\mathbf{S}}_2^{-1}\right]\mathbf{b}_N \\
&= \left[\overleftrightarrow{\mathbf{P}}_2^{-1} + \gamma\left(\overleftrightarrow{\mathbf{S}}_2^{-1}\overleftrightarrow{\mathbf{S}}_1 - \overleftrightarrow{\mathbf{P}}_2^{-1}\overleftrightarrow{\mathbf{P}}_1\right)\overleftrightarrow{\mathbf{L}}_1^{-1}\left(\overleftrightarrow{\mathbf{L}} - \overleftrightarrow{\mathbf{M}}\overleftrightarrow{\mathbf{P}}_2^{-1}\overleftrightarrow{\mathbf{P}}_1\right)^{-1}\overleftrightarrow{\mathbf{M}}\overleftrightarrow{\mathbf{P}}_2^{-1}\right]\mathbf{b}_T \\
&+ \left[\left(\overleftrightarrow{\mathbf{S}}_2^{-1}\overleftrightarrow{\mathbf{S}}_3 - \overleftrightarrow{\mathbf{P}}_2^{-1}\overleftrightarrow{\mathbf{P}}_3\right) - \gamma\left(\overleftrightarrow{\mathbf{S}}_2^{-1}\overleftrightarrow{\mathbf{S}}_1 - \overleftrightarrow{\mathbf{P}}_2^{-1}\overleftrightarrow{\mathbf{P}}_1\right)\overleftrightarrow{\mathbf{L}}_1^{-1}\overleftrightarrow{\mathbf{L}}_2\right]\mathbf{I}_f. \quad (10)
\end{aligned}$$

In the limit of $\mathbf{I}_f = 0$, Eq. (10) recovers equation (15) from [10]. Ref. [10] gives a rigorous proof, in the cylindrical limit, that this boundary condition does result in the correct eigenvalue for the RWM.

In principle, all the coefficient matrices from Eq. (10) can be straightforwardly computed by an eddy current solver. However, this may not always be efficient, since a large amount of matrices manipulations are required. For a 3D structure with complex geometry, some of the intermediate operations involve inversions and multiplications of large-dimension matrices (normally $N \gg M, K$). We propose a better procedure by noticing that Eq. (10) suggests a linear matrix relation between $\mathbf{b}_N$, $\mathbf{b}_T$ and $\mathbf{I}_f$ with respect to γ. We re-write this relation as

$$\left(\overleftrightarrow{\mathbf{A}}_{0N} + \gamma\overleftrightarrow{\mathbf{A}}_{1N}\right)\mathbf{b}_N + \left(\overleftrightarrow{\mathbf{A}}_{0T} + \gamma\overleftrightarrow{\mathbf{A}}_{1T}\right)\mathbf{b}_T + \left(\overleftrightarrow{\mathbf{A}}_{0f} + \gamma\overleftrightarrow{\mathbf{A}}_{1f}\right)\mathbf{I}_f = 0, \quad (11)$$

where all the coefficient matrices have relatively small dimensions ($M \times M$ or $M \times K$). One of the matrices, for instance $\overleftrightarrow{\mathbf{A}}_{0T}$, can be set to be an identity matrix. The remaining matrices can be found numerically in two steps using an eddy current solver.

First, assuming a vanishing coil current $\mathbf{I}_f = 0$, and assuming a set of M linearly independent equivalent surface currents $\mathbf{I}_{\text{eqv}}$, the eddy current solver computes the corresponding total normal field $\overleftrightarrow{\mathbf{b}}_N$ (now a $M \times M$ matrix) on the coupling surface, and the total tangential field $\overleftrightarrow{\mathbf{b}}_T$ (a $M \times M$ matrix) *just outside* the coupling surface, following Eqs. (1)-(3). [Note that the tangential field $\mathbf{b}_T$ experiences a jump across the coupling surface due to the presence of the surface current $\mathbf{I}_{\text{eqv}}$ on the control surface.] Repeating the above exercise for three given (distinct) γ values yields three matrices equations (11) for three unknown matrix coefficients $(\overleftrightarrow{\mathbf{A}}_{0N}, \overleftrightarrow{\mathbf{A}}_{1N}, \overleftrightarrow{\mathbf{A}}_{1T})$ of dimension $M \times M$, which can be easily solved to obtain these matrix coefficients.

Knowing the above matrix coefficients $(\overleftrightarrow{\mathbf{A}}_{0N}, \overleftrightarrow{\mathbf{A}}_{1N}, \overleftrightarrow{\mathbf{A}}_{1T})$, the second step assumes an arbitrary equivalent surface current $\mathbf{I}_{\text{eqv}}$, and a set of K basis vectors for $\mathbf{I}_f$, and solve the forcing eddy current problem again for $\mathbf{b}_N$ and $\mathbf{b}_T$. The resulting fields are inserted into Eq. (11) to find the columns of the matrix coefficients $\overleftrightarrow{\mathbf{A}}_{0f}$ and $\overleftrightarrow{\mathbf{A}}_{1f}$, of

dimension $M \times K$. This procedure has to be repeated for two values of γ, with $\gamma_1 = 0$ and $\gamma_2 \neq 0$ respectively.

2.2. Sensor flux

For both RFA and feedback studies, a set of L sensor coils, located in the vacuum region, are used to detect the (radial or tangential) magnetic flux, denoted here by ψ_s of dimension $L \times 1$. ψ_s can be computed according to

$$\psi_s = \overleftrightarrow{\mathbf{M}}_1 \mathbf{I} + \overleftrightarrow{\mathbf{M}}_2 \mathbf{I}_{\text{eqv}} + \overleftrightarrow{\mathbf{M}}_3 \mathbf{I}_f, \tag{12}$$

where $\overleftrightarrow{\mathbf{M}}_1$, $\overleftrightarrow{\mathbf{M}}_2$ and $\overleftrightarrow{\mathbf{M}}_3$ are mutual inductance matrices between the corresponding current and the sensor coils. We combine Eq. (12) with Eqs. (2) and (6) to eliminate subsequently the currents $\mathbf{I}_{\text{eqv}}$ and $\mathbf{I}_f$. A straightforward algebraic manipulation leads to a linear relation of the form

$$\psi_s = \left(\overleftrightarrow{\mathbf{D}}_{0N} + \gamma \overleftrightarrow{\mathbf{D}}_{1N}\right) \mathbf{b}_N + \gamma \overleftrightarrow{\mathbf{D}}_{1T} \mathbf{b}_T + \left(\overleftrightarrow{\mathbf{D}}_{0f} + \gamma \overleftrightarrow{\mathbf{D}}_{1f}\right) \mathbf{I}_f, \tag{13}$$

where

$$\begin{aligned}
\overleftrightarrow{\mathbf{D}}_{0N} &\equiv \overleftrightarrow{\mathbf{M}}_2 \overleftrightarrow{\mathbf{S}}_2^{-1}, \\
\overleftrightarrow{\mathbf{D}}_{1N} &\equiv -\left(\overleftrightarrow{\mathbf{M}}_1 - \overleftrightarrow{\mathbf{M}}_2 \overleftrightarrow{\mathbf{S}}_2^{-1} \overleftrightarrow{\mathbf{S}}_1\right) \overleftrightarrow{\mathbf{L}}_1^{-1} \left(\overleftrightarrow{\mathbf{L}} - \overleftrightarrow{\mathbf{M}} \overleftrightarrow{\mathbf{S}}_2^{-1} \overleftrightarrow{\mathbf{S}}_1\right)^{-1} \overleftrightarrow{\mathbf{M}} \overleftrightarrow{\mathbf{S}}_2^{-1}, \\
\overleftrightarrow{\mathbf{D}}_{1T} &\equiv \left(\overleftrightarrow{\mathbf{M}}_1 - \overleftrightarrow{\mathbf{M}}_2 \overleftrightarrow{\mathbf{S}}_2^{-1} \overleftrightarrow{\mathbf{S}}_1\right) \overleftrightarrow{\mathbf{L}}_1^{-1} \left(\overleftrightarrow{\mathbf{L}} - \overleftrightarrow{\mathbf{M}} \overleftrightarrow{\mathbf{P}}_2^{-1} \overleftrightarrow{\mathbf{P}}_1\right)^{-1} \overleftrightarrow{\mathbf{M}} \overleftrightarrow{\mathbf{P}}_2^{-1}, \\
\overleftrightarrow{\mathbf{D}}_{0f} &\equiv \overleftrightarrow{\mathbf{M}}_3 - \overleftrightarrow{\mathbf{M}}_2 \overleftrightarrow{\mathbf{S}}_2^{-1} \overleftrightarrow{\mathbf{S}}_3, \\
\overleftrightarrow{\mathbf{D}}_{1f} &\equiv -\left(\overleftrightarrow{\mathbf{M}}_1 - \overleftrightarrow{\mathbf{M}}_2 \overleftrightarrow{\mathbf{S}}_2^{-1} \overleftrightarrow{\mathbf{S}}_1\right) \overleftrightarrow{\mathbf{L}}_1^{-1} \overleftrightarrow{\mathbf{L}}_2.
\end{aligned}$$

The matrices $\overleftrightarrow{\mathbf{D}}_{0N}, \overleftrightarrow{\mathbf{D}}_{1N}$ and $\overleftrightarrow{\mathbf{D}}_{1T}$ have dimension $L \times M$, and the matrices $\overleftrightarrow{\mathbf{D}}_{0f}$ and $\overleftrightarrow{\mathbf{D}}_{1f}$ have dimension $L \times K$. Again we are not interested in the exact definition of these matrices, since we shall compute them numerically, in a similar manner as we compute the coupling matrices for the boundary condition (11). We again follow two steps.

First, assuming a vanishing coil current $\mathbf{I}_f = 0$, and a set of M independent equivalent surface currents $\mathbf{I}_{\text{eqv}}$, the eddy current code produces three sets of matrix data $(\overleftrightarrow{\mathbf{b}}_{jN}, \overleftrightarrow{\mathbf{b}}_{jT}, \overleftrightarrow{\psi}_{js})_{j=1,2,3}$, for three distinct γ values $\gamma_j, j = 1, 2, 3$ respectively. The matrices for the field have dimension $M \times M$, the matrices for the flux have dimension $L \times M$. These three sets of data, satisfying Eq. (13) (in which $\mathbf{I}_f = 0$), create a system of matrix equations, that can be solved to find $\overleftrightarrow{\mathbf{D}}_{0N}, \overleftrightarrow{\mathbf{D}}_{1N}$ and $\overleftrightarrow{\mathbf{D}}_{1T}$.

At the second step, assuming an arbitrary equivalent surface current $\mathbf{I}_{\text{eqv}}$, and a set of K basis vectors for $\mathbf{I}_f$, and solve the forcing eddy current problem again for $\mathbf{b}_N$, $\mathbf{b}_T$ and ψ_s, at two distinct eigenvalues $\gamma_1 = 0$ and $\gamma_2 \neq 0$. The resulting fields are inserted into Eq. (13) to find the columns of the matrix coefficients $\overleftrightarrow{\mathbf{D}}_{0f}$ and $\overleftrightarrow{\mathbf{D}}_{1f}$, using the matrices $\overleftrightarrow{\mathbf{D}}_{0N}, \overleftrightarrow{\mathbf{D}}_{1N}$ and $\overleftrightarrow{\mathbf{D}}_{1T}$ computed at the first step.

2.3. Remarks and brief summary

We notice that the whole coupling procedure described above may seem sophisticated. However, the enormous benefit that we gain is to have the full access to the MHD and kinetic physics of the RWM without compromising the effects of 3D structures. It will be even more beneficial if we consider non-linear MHD physics.

It may also be possible to improve the forward coupling scheme described in [10], by including the plasma inertia and rotation effects (dynamic response) into the coupling matrices for the eddy current code. These coupling matrices, generally depending non-linearly on the eigenvalue γ, can be arranged into a set of linear boundary conditions for the eddy current solver, by applying a matrix-based, low-order Padé approximation for the plasma dynamic response. The drawbacks of this approach are: (i) the plasma dynamics is included in the final modelling in an approximate way (Padé approximation), whilst the backward coupling procedure, described in this Section, takes into account the *exact* response of the conducting structures (up to the discretisation error); (ii) it may not always be possible to "transfer" the full plasma dynamics via the magnetic field alone. One example is a resistive plasma.

The drawbacks of the backward coupling scheme, which are in turn the advantages of the forward coupling scheme, are (i) complexity in taking into account the geometrical coupling of various toroidal mode numbers [10]. This coupling occurs due to 3D features of the conducting structures, even with the linear MHD approximation in an axi-symmetric system; (ii) less flexibility in performing direct closed-loop simulations with an arbitrary choice of controllers, control power supplies, and control performance specifications. A full solution to the first issue requires computing mutual coupling matrices between different n's, which can be performed using the electromagnetic code. The second issue can be partially resolved by decoupling the feedback problem into two separate problems, namely the construction of the plasma response model [13], and the model-based controller design.

We summarise this Section by pointing out how to apply equations (11) and (13) to three of the RWM related problems. In all the cases, the effects of plasma inertia, flow, and damping physics are included.

In order to compute the passive growth rate of the RWM, we set $\mathbf{I}_f = 0$ in Eq. (11), and simply use this equation as the boundary condition for the MHD solver, where the computational boundary is the coupling surface, on which the linear relation (11) between $\mathbf{b}_N$ and $\mathbf{b}_T$ is computed. Ref. [10] shows that this boundary condition indeed results in the correct eigenvalue for the RWM.

In order to compute the RFA response of a stable plasma, we set $\mathbf{I}_f$ at a given value, and $\gamma = i\omega_{\text{ext}}$ at a given frequency ω_{ext}, and solve a forcing problem, where the source term $\mathbf{I}_f$ enters into the equations via the boundary condition (11). The solution of the forcing problem gives the total magnetic fields $\mathbf{b}_N$ and $\mathbf{b}_T$ at the computational boundary, which are then used to evaluate the sensor coil flux ψ_s via Eq. (13). The same procedure can also be used to construct the plasma response model for an unstable

plasma, for the purpose of feedback stabilisation of the RWM [13].

In the third case, we wish to compute directly the growth rate of the RWM in the presence of feedback (the closed-loop eigenvalue problem). The vectors $\mathbf{I}_f$ and ψ_s have to be included in the MHD solver as additional solution variables. Besides the boundary condition (11), the MHD equations are solved together with the sensor equation (13) and an additional set of equations for the feedback coils (the feedback law)

$$\mathbf{I}_f = -\overleftrightarrow{\mathbf{G}}(\gamma)\psi_s, \tag{14}$$

where $\overleftrightarrow{\mathbf{G}}$ is the feedback gain matrix, which generally depends on the eigenvalue γ. For a PID (proportional, derivative and integral) controller, it is easy to recast Eq. (14) as a linear relation with respect to γ.

The above feedback law (14) assumes the so-called flux-to-current control. If instead, the applied voltages $\mathbf{V}_f$ (of dimension $K \times 1$) to the resistance-inductance feedback coils are the control variable, we have a flux-to-voltage control

$$\mathbf{V}_f = -\overleftrightarrow{\mathbf{G}}(\gamma)\psi_s, \tag{15}$$

In this case, by assuming

$$\mathbf{V}_f = \gamma\left(\overleftrightarrow{\mathbf{Q}}_1\mathbf{I} + \overleftrightarrow{\mathbf{Q}}_2\mathbf{I}_{\mathrm{eqv}} + \overleftrightarrow{\mathbf{Q}}_3\mathbf{I}_f\right) + \overleftrightarrow{\mathbf{R}}_f\mathbf{I}_f, \tag{16}$$

and by combining Eq. (16) with Eqs. (2) and (6) again, we can arrive at two sets of linear relations

$$\mathbf{V}_f = \gamma\overleftrightarrow{\mathbf{U}}_{1N}\mathbf{b}_N + \gamma\mathbf{b}_Q + \left(\overleftrightarrow{\mathbf{R}}_f + \overleftrightarrow{\mathbf{U}}_{1f}\right)\mathbf{I}_f, \tag{17}$$

$$\mathbf{b}_Q = \gamma\left(\overleftrightarrow{\mathbf{U}}_{2N}\mathbf{b}_N + \overleftrightarrow{\mathbf{U}}_{2T}\mathbf{b}_T + \overleftrightarrow{\mathbf{U}}_{2f}\mathbf{I}_f\right), \tag{18}$$

where the matrix coefficients are again computed using the similar two-step procedure as for the boundary condition and the sensor flux equations.

Equations (15), (17), (18) and (11), together with MHD equations, form a closed system to study the RWM stability in the presence of voltage control coils.

3. CarMa test results

The backward coupling scheme, described in the previous Section, is realised in a new version of the CarMa code. This Section reports results on a test example. We choose a numerical equilibrium with aspect ratio 5, circular poloidal cross section, and the profiles for the safety factor q and the plasma pressure shown in Fig. 1. For the $n = 1$ RWM that we study here, only one rational surface $q = 2$ is present inside the plasma. We assume a uniform rotation profile, and an analytic (normalised) plasma density profile

$$\rho = 1 - 0.7\psi_p,$$

where ψ_p is the normalised equilibrium poloidal flux ($\psi_p = 0$ corresponds to the plasma magnetic axis, and $\psi_p = 1$ corresponds to the plasma surface). A conformal (i.e. circular) resistive wall is placed at 1.3 times the plasma minor radius. The

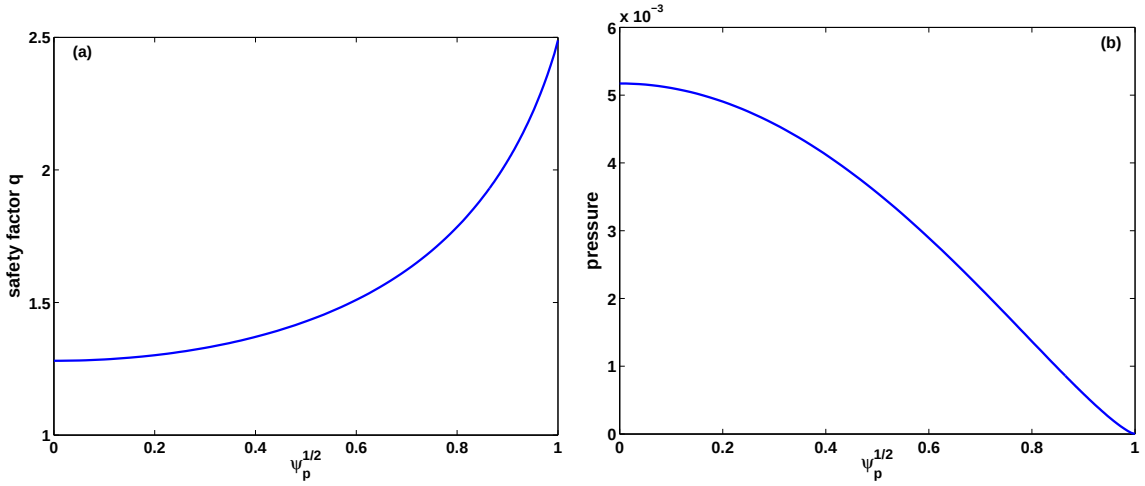

Figure 1. Equilibrium profiles for (a) the safety factor q, and (b) the plasma pressure, normalised by the factor B_0^2/μ_0, with B_0 the vacuum toroidal field on the magnetic axis.

resistive wall mode instability in this case is largely current-driven. For the purpose of benchmarking the code, and illustrating the synergistic effects of both damping physics and 3D conductors, we restrict ourselves by studying only the stability problem.

Besides the Alfvénic and acoustic wave damping, which is automatically included in the code (via MHD terms), we consider two additional pieces of damping physics. The first is the parallel sound wave damping model (SD), described in detail in Refs. [14, 15]. The model introduces a numerically adjustable coefficient $\kappa_{||}$, which prescribes the strength of the damping. We set $\kappa_{||} = 1.5$, which normally corresponds to a strong damping. Our previous comparison of modelling results with experiments [15] suggests that a strong parallel sound wave damping model is more appropriate than a weak damping, in describing the RWM dynamics in tokamak plasmas.

The second damping model is the self-consistent, full toroidal drift kinetic model (KD), proposed and implemented in the MARS-K code [1]. This is a full physics model without any numerically adjustable parameters. In this model, the damping comes from the mode resonance either with bounce motion of both passing and trapped thermal ions at fast plasma rotation (the plasma $E \times B$ rotation frequency ω_E comparible with the ion bounce frequency ω_b^i), or with the magnetic precession drift of trapped thermal ions and electrons at slow plasma rotation ($\omega_E < \min(\omega_b^i, \omega_{*i})$, with ω_{*i} being the ion diamagnetic drift frequency). Since our purpose here is *not* a detailed investigation of various kinetic damping physics, we consider only the precession drift resonances, and neglect the bounce resonances, as well as other physics such as the collisionality effects.

Figure 2 compares the RWM eigenvalues versus ω_E, assuming either the parallel sound wave damping or the drift kinetic damping model. A 2D complete wall is used. In this case we can either run MARS-K to compute the mode stability directly, or run the CarMa code, where the frequency response of the 2D wall is first computed using

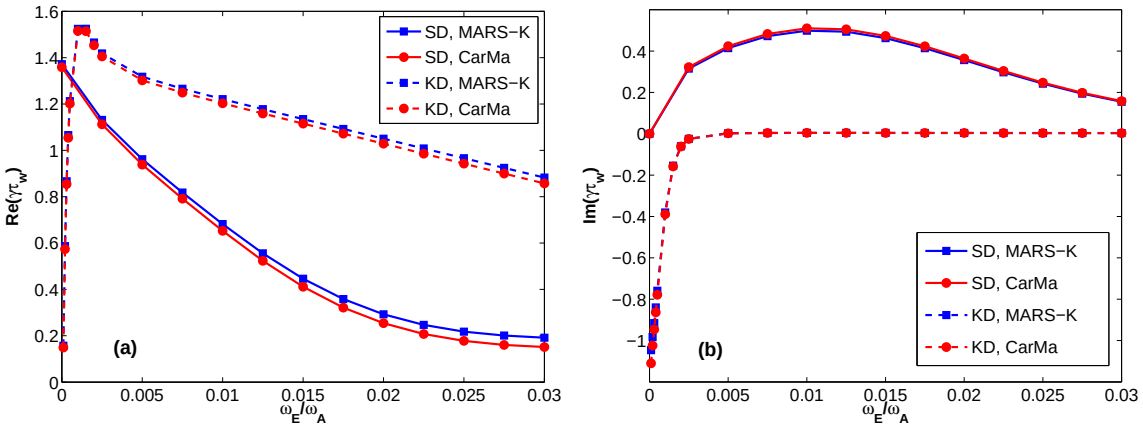

Figure 2. Comparison of the (a) real, and (b) imaginary parts of the RWM eigenvalue, computed by MARS-K ("square") and CarMa ("dot"). Both sound wave damping (solid) and self-consistent drift kinetic damping models are considered. A 2D complete wall is considered.

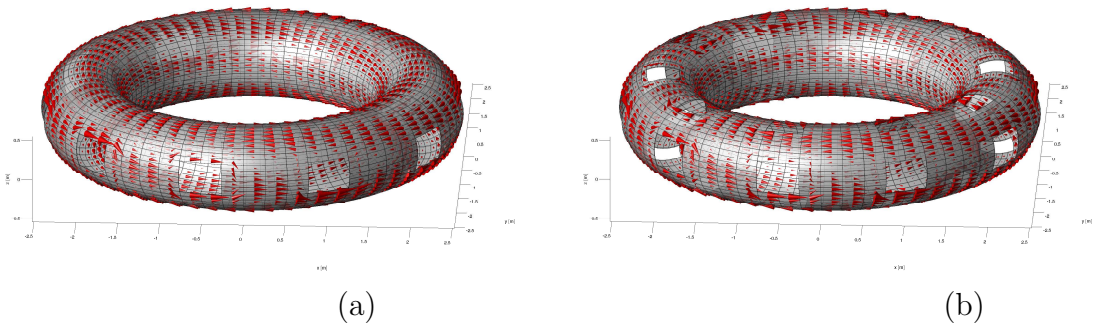

Figure 3. Two 3D wall models ((a) - model A, (b) - model B) with holes. Shown also the eddy current flow pattern on the walls, induced by the unstable RWM without the plasma rotation.

the eddy current code, and then used as the boundary condition for solving the MHD equations together with kinetic terms. As expected, two codes give almost identical results, for both the mode growth rates and the mode frequency. A minor difference results from the numerical inaccuracy in 3D discretisation of the 2D wall, as well as from computing the response matrices. These results benchmark the new implementation of the CarMa code.

Now we consider the rotational and kinetic stabilisation of the RWM in the presence of a 3D wall. Two wall models (A and B) are chosen, as shown in Fig. 3. The model A has holes at the outboard mid-plane along the toroidal angle. The model B has more holes, on the top and bottom of the wall, allowing the mode to be more unstable.

Figure 4 compares the computed RWM eigenvalue with different wall models. The parallel sound wave damping model is considered. For this specific example, no full stabilisation of the mode is found, even at the ω_E value reaching 3% of the Alfvén

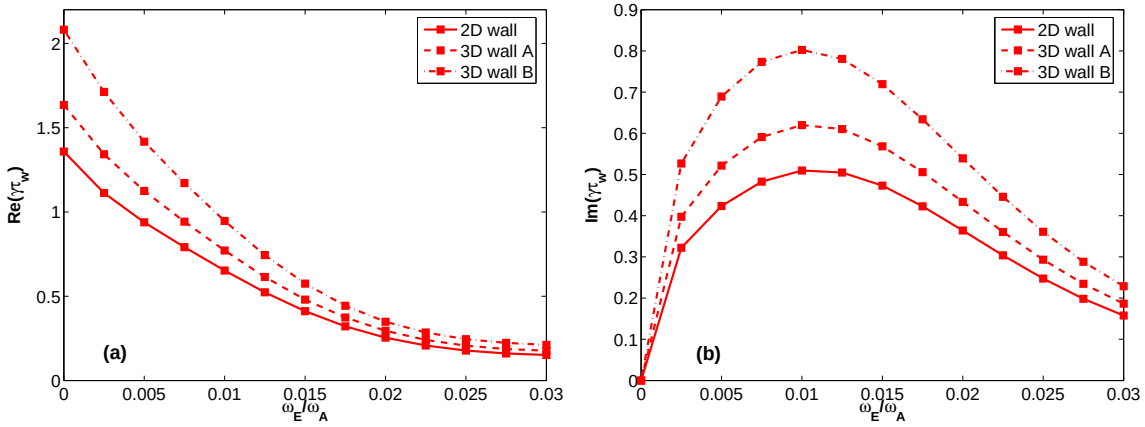

Figure 4. Comparison of the (a) real, and (b) imaginary parts of the RWM eigenvalue, computed by CarMa assuming a 2D compete wall model (solid), and with two 3D wall models with holes (dashed and dash-dotted). The sound wave damping model is considered.

frequency. The mode is more unstable with less complete walls, as expected. It is interesting, though, to notice that the mode frequency also increases with more holes in the wall. At fast plasma rotation ($\omega_E \simeq 0.03\omega_A$), the mode frequency tends to vanish, and the mode growth rate with 3D walls tends to converge to the 2D wall value. This is not surprising, since at zero mode frequency and at the mode stability margin, the eddy current in the wall would vanish. Therefore, the 3D effects of the wall disappear at the stability boundary. Effectively we obtain the same marginal stability condition (if that occurs) for both 2D and 3D walls. We emphasise that this is valid only if the mode frequency also vanishes at the stability margin. Another example of such a condition is the RWM feedback stabilisation in a non-rotating plasma. Without additional (kinetic) damping, the closed-loop growth rate of the mode is normally real. Hence the same feedback loop that brings the RWM to a marginal stability with 2D walls, should also do the same with 3D walls.

Figure 5 again compares the computed RWM eigenvalue with different wall models, but with the self-consistent drift kinetic model. Again we notice that the mode is more unstable with more holes in the wall, through the whole range of the rotation frequency considered here. 3D walls also enhance the mode rotation with respect to the wall. It is interesting to notice that the kinetic effects (thermal particle precessional drift resonances with the mode in this case) occur strongly at very slow rotation frequency $\omega_E \sim 10^{-4}\omega_A$, for all wall models. This frequency range agrees with that of the thermal particle precession drift frequency, as shown in Fig. 6. The mode, which has a frequency close to the ω_E frequency in the plasma frame, due to the Doppler shift, experiences a strong resonance damping with the trapped thermal particles in this region. For this specific example, the drift kinetic effects can bring a full stabilisation of the mode at vanishing plasma rotation. It should be noted that bounce resonance effects (not included in this test study) would be expected to be significant at ω_E the order of

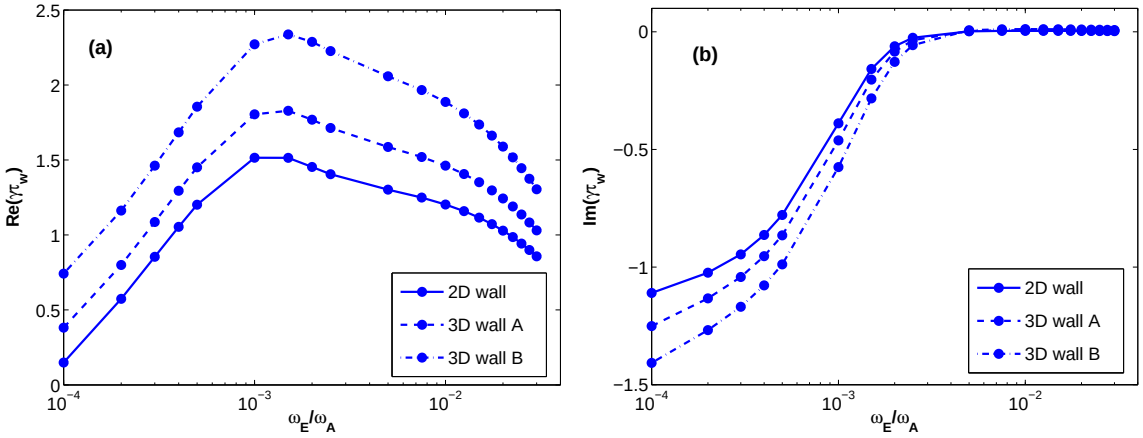

Figure 5. Comparison of the (a) real, and (b) imaginary parts of the RWM eigenvalue, computed by CarMa assuming a 2D compete wall model (solid), and with two 3D wall models with holes (dashed and dash-dotted). The self-consistent drift kinetic damping model is considered.

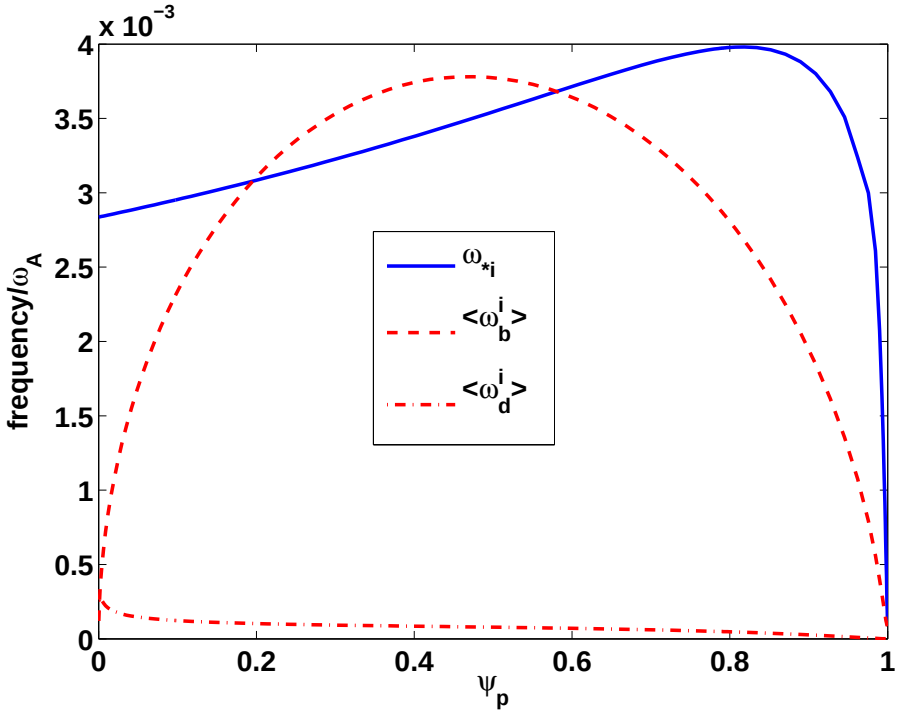

Figure 6. The radial profile of the ion-diamagnetic frequency ω_{*i}, the bounce frequency ω_b^i, and the magnetic drift precession frequency ω_d^i, of trapped thermal ions. The latter two frequencies are averaged over the particle (Maxwellian) distribution function.

$10^{-3}\omega_A$. In this frequency range, additional damping is expected thanks to the match between the mode frequency (in the plasma frame) and the thermal particle bounce frequency shown in Fig. 6.

4. Conclusion

We have proposed a rigorous approach to study the stability, control and resonant response of the RWM, in the presence of plasma inertia, various damping physics associated with the mode in a rotating plasma, as well as 3D conducting structures (walls and coils). Since this approach utilises boundary conditions, derived from the electromagnetic eddy current computation, to the full toroidal MHD-kinetic hybrid computation, all the relevant mode damping physics, such as the Alfvén and sound wave continuum damping, the parallel sound wave ion Landau damping, or the drift kinetic particle-wave resonance damping, can be easily incorporated into the numerical study.

A new implementation of the CarMa code is reported, based on this approach. A benchmark test shows the correctness and flexibility of the new implementation.

The results on the test example show that the major effect of 3D openings (holes) in the conducting wall is to further destabilise the mode, compared with the case with a complete wall. This destabilisation persists in various mode damping regimes. At the same time, the mode rotation (with respect to the wall) is also generally enhanced by the presence of 3D features in the wall. Finally, it is not surprising though interesting that, if a damping mechanism brings the mode to a stability margin with vanishing frequency, the 3D wall effects disappear. In this case, the mode marginal stability is entirely determined by the "interior" properties of the plasma.

Acknowledgments

This work was partly funded by the United Kingdom Engineering and Physical Sciences Research Council and by the European Communities under the contract of Association between EURATOM and UKAEA. The views and opinions expressed herein do not necessarily reflect those of the European Commission.

References

[1] Yueqiang Liu *et al* 2008 *Phys. Plasmas* **15** 112503
[2] Yueqiang Liu *et al* 2000 *Phys. Plasmas* **7** 3681
[3] Strumberger E *et al* 2005 *Nucl. Fusion* **45** 1156
[4] Albanese R *et al* 2008 *IEEE Trans. Magn.* **44** 1654
[5] Portone A *et al* 2008 *Plasma Phys. Control. Fusion* **50** 085004
[6] Bialek J *et al* 2008 *Phys. Plasmas* **8** 2170
[7] Merkel P *et al* 2006 *21st IAEA Fusion Energy Conf. 2006 (Chengdu, China)* (Vienna: IAEA) TH/P3-8
[8] Villone F *et al* 2008 *Phys. Review Lett.* **100** 255005
[9] Albanese R and Rubinacci G 1998 *Advances in Imaging and Electron Physics* **102** 1
[10] Yueqiang Liu *et al* 2008 *Phys. Plasmas* **15** 072516
[11] Guazzotto L *et al* 2008 *Phys. Plasmas* **15** 072503
[12] Smith S P and Jardin S C 2008 *Phys. Plasmas* **15** 080701
[13] Yueqiang Liu 2007 *Comp. Phys. Communic.* **176** 161

[14] Chu M S *et al* 1995 *Phys. Plasmas* **2** 2236
[15] Liu Y Q *et al* 2005 *Nucl. Fusion* **45** 1131